Essential Readings in Light Metals: Cast Shop for Aluminum Production.
Edited by John F. Grandfield and Dmitry G. Eskin.

COLD CRACKING DURING DIRECT-CHILL CASTING

D.G. Eskin[1,2], M. Lalpoor[2], L. Katgerman[3]
[1]Materials innovation institute, Mekelweg 2, 2628 CD Delft, The Netherlands
[2]Brunel University, BCAST, Uxbridge, UB8 3PH, U.K.
[3]Delft University of Technology, Department of Materials Science and Engineering, Mekelweg 2, 2628 CD Delft, The Netherlands

Keywords: aluminum alloys, DC casting, cold cracking, fracture, thermomechanical simulation

Abstract

Cold cracking phenomenon is the least studied, yet very important defect occurring during direct chill casting. The spontaneous nature of this defect makes its systematic study almost impossible, and the computer simulation of the thermomechanical behavior of the ingot during its cooling after the end of solidification requires constitutive parameters of high-strength aluminum alloys in the as-cast condition, which are not readily available. In this paper we describe constitutive behavior of high strength 7xxx series aluminum alloys in the as-cast condition based on experimentally measured tensile properties at different strain rates and temperatures, plane strain fracture toughness at different temperatures, and thermal contraction. In addition, fracture and structure of the specimens and real cold-cracked billets are examined. As a result a fracture-mechanics-based criterion of cold cracking is suggested based on the critical crack length, and is validated upon pilot-scale billet casting.

Introduction

7xxx series aluminum alloys are highly prone to cracking at different stages of solidification and cooling during the direct chill casting process. The susceptibility to cracking is on the one hand due to the precipitation of low melting point brittle intermetallics on grain boundaries and interdendritic spaces [1, 2], and on the other hand to the development of high residual thermal stresses [3]. Above the solidus, the low strength of the low melting point nonequilibrium eutectics and intermetallics provide potential sites for hot tearing [4]. Further propagation of such cracks under the tensile stress fields that develop to some critical levels below the solidus may result in catastrophic failure of the ingot in the solid state; cold cracking [5]. What makes the material even more susceptible to cold cracking is the sever loss in ductility upon cooling after the end of solidification [6]. Although the specific microstructure of the material in the as-cast condition provides potential crack sites for hot and cold cracking, the stress development in the ingots during the casting is brought about by the non-homogenous cooling conditions and the poor thermophysical properties of the material. Relatively higher coefficient of thermal expansion and the lower thermal conductivity of some of 7xxx series alloys compared to other aluminum alloys [7] result in steep temperature gradients and consequently high thermal stresses appear. In order to predict the cold cracking phenomenon in high strength aluminum alloys, a true understanding of the residual thermal stress development during the casting is required. In the 1950s, thermal stresses were calculated analytically by Livanov [8] for ingots with various geometries. He even established a criterion based on numerous experimental trials under different casting conditions. With the development of computer simulations, however the costly casting trials were replaced by numerical calculations. Numerical simulations helped to reveal the critical locations in the casting and stages of casting over which high tensile stresses appear and trigger cold cracking [9, 10]. The next step was the application of fracture mechanics to assess the critical crack/void size required for the occurrence of catastrophic failure. Boender *et al.* [11] and O. Ludwig *et al.* [12] applied the fracture mechanics to the results of the thermomechanical simulations with the aim to find the critical locations in the ingots where the brittle fracture is more probable to occur. Although precious from technical point of view, these results were not validated upon casting trials to check how closely they relate to the actual crack sizes.

The computer simulation results may be more reliable if the constitutive parameters, mechanical properties and the plane strain fracture toughness of the material are gained from the as-cast material. As the 7xxx series aluminum alloys are mainly used in the fully hardened state, very little research has been performed on their properties in the genuine as-cast condition and the properties of the material in the heat treated states would not represent the as-cast conditions [6]. Even in the homogenized [13] or stress relieved [14] states, the constitutive properties are considerably different than the as-cast ones, which may lead to unreliable calculated stress values and eventually critical crack size estimations. In order to prevent all these problems, the constitutive parameters, mechanical properties and the plane strain fracture toughness of the material in the genuine as-cast condition are required. In this study, we report the results of the thermomechanical tests for an AA7050 alloy, which were used as input data for computer simulations. Having applied the fracture mechanics to the results of the thermomechanical simulations, the critical crack sizes required for catastrophic failure were calculated for the entire billets conditions. The simulation results were eventually validated upon pilot scale casting trials on another typical 7xxx alloy which is highly prone to both hot and cold cracking.

Experimental procedure

The material used in this research work was extracted from an AA7050 billet produced by DC casting with a conventional mold from the melt that was degassed in the furnace, and supplied by Corus-Netherlands (IJmuiden). Chemical composition of the alloy in terms of wt% is as follows: Zn: 6.3, Mg: 2.42, Cu: 2.49, Zr: 0.098, Ti: 0.03, Fe: 0.07, Si: 0.04, Mn: 0.04 and Cr: <0.01.

Tensile mechanical properties of the as-cast samples were measured using a Gleeble-1500 thermomechanical simulator. Samples were cut from a cylindrical billet with a diameter of 255 mm along its radial direction. Tensile specimens were heated through the Joule effect at a rate of 10 K/s, kept for 10 seconds and then uniaxially deformed at three strain rates of 10^{-2}, 10^{-3} and 10^{-4} s^{-1}. The range of strain rates was chosen to resemble those typical of DC casting [15]. Mechanical properties were measured from room temperature to 400 °C at 100 °C steps. Four samples were tested for each specific temperature and strain rate combination, and the average values are reported.

In order to assess the critical crack size leading to catastrophic failure, plane strain fracture toughness tests were performed from room temperature to 200 °C following ASTM-E399 regulations. The samples prepared based on the dimensional proportions mentioned in the standard were locally polished around the chevron notch to be able to follow and accurately measure the fatigue crack length. Samples were then fatigue pre-cracked at room temperature to reach the total crack length of 15 mm (including the chevron notch length of 13 mm). Loading rate was chosen in such a way to keep the stress intensity within the range of 0.55–2.75 MPa $m^{1/2}$ s^{-1}. At higher temperatures, samples were first covered with a ceramic coating for insulation and preventing a sudden temperature fall (temperature tolerance was ±10°C) and then kept at desired temperatures in an oven for 20 minutes.

Experimental results and discussion

Figures 1 and 2 show the effect of temperature on the frature strength and ductility (% reduction in area). Due to very low ductility the fracture strength can be accepted as the yield strength. The fracture strength reaches 266 MPa at room temperature and falls to 23 MPa as the temperature increases to 400 ºC. The fracture strength increases as the temperature decreases in a linear manner. As temperature falls below 400 ºC, the material starts to behave even more brittle and shows less ductility. The alloy loses its ductility completely below 200 ºC, which is accompanied by a higher fracture strength.

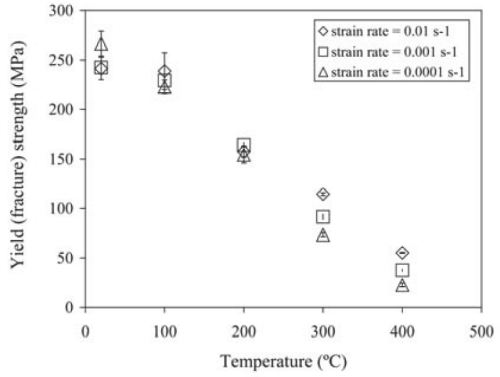

Figure 1. Average yield (fracture) strength of the AA7050 samples at different temperatures and strain rates [16].

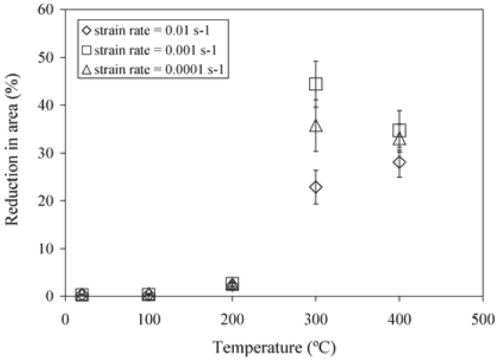

Figure 2. Ductility of the AA7050 samples at different temperatures and strain rates [16].

The effect of strain rate on the flow stress of the AA7050 alloy at the true strain 0.002 is shown in Figure 3. At high temperatures (300 and 400 ºC) the flow stress increases as the deformation rate increases, but at lower temperatures (beginning at 200 ºC) the material behavior becomes strain-rate independent.

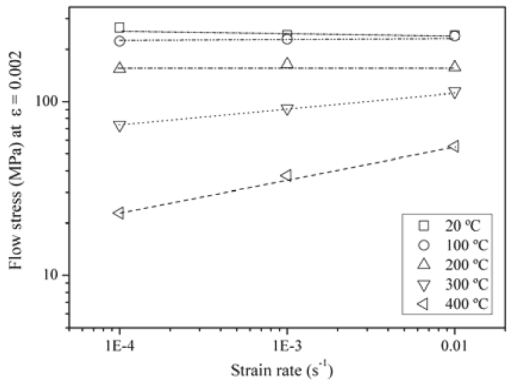

Figure 3. The effect of strain rate on the flow stress at ε =0.002 at different temperatures [16].

Plane strain fracture toughness values (K_{Ic}) values from room temperature to 200 °C were calculated using the load-displacement curves and are presented in Figure 4. As can be seen there is a slight decrease in K_{Ic} values with increasing the temperature. But taking the error values into account, the differences are insignificant. Above 200°C, plane strain conditions were not valid any more, mainly because of the fall in the yield strength at that temperature (154 MPa at 200 °C to 73 MPa at 300 °C).

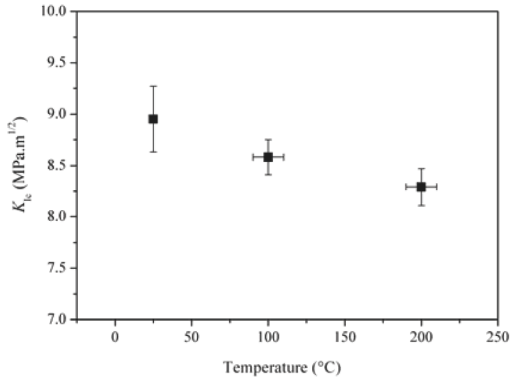

Figure 4. Plane strain fracture toughness (K_{Ic}) values measured for the as-cast AA7050 (DC-cast) alloy from room temperature to 200°C [5].

The comparison of the K_{Ic} results gained for the genuine as-cast material here with the minimum K_{Ic} for the material in the precipitation hardened state (20.9–27.5 MPa·$m^{1/2}$, at room temperature [7]) shows how brittle the material is under as-cast conditions.

Constitutive parameters

In order to simulate the DC-casting process from solidus temperature to room temperature suitable equations describing the

material's mechanical behavior are required. One approach is the extended Ludwik equation [17]:

$$\sigma = K(T)(\varepsilon_p + \varepsilon_p^0)^{n(T)}(\dot{\varepsilon}_p)^{m(T)} \quad (1)$$

K(T) is the consistency of the alloy, n(T) is the strain hardening coefficient, m(T) is the strain rate sensitivity, and ε_p^0 is a constant equal to 0.001 [12]. The true stress-strain curves of the material were fitted to Equation 1 to determine $K(T)$, $n(T)$ and $m(T)$, and the results are presented in Figures 5 through 7. In the same graphs, the reference data gained from the stress relieved samples [14] and the homogenized samples [18] are also reported. As can be seen in Figure 5, the consistency of the genuine as-cast material falls in a continous manner with temperature. In homogenized and stress relieved samples however, it passes through a plateau and then falls with increasing the temperature. It is noticeable that the main difference occurs at lower temperatures were the material is more prone to cracking due to its extreme brittleness. The same trend is observed for strain hardening coefficient of the alloy (Figure 6), although the difference in the results appears to be higher at elevated temperatures especially in the stress relieved material. Stress rate sensitivity values are in a relatively good agreement at lower temperatures, but the difference becomes larger at higher temperatures (Figure 7). m values turn to zero below 200 ºC in agreement with the strain rate independent behavior shown in Figure 3.

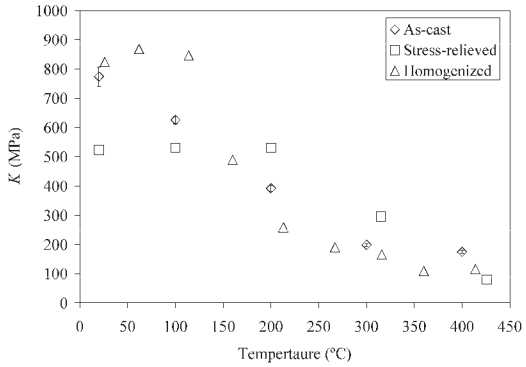

Figure 5. Consistency of the AA7050 alloy gained from various samples: as-cast (this study), stress relieved [14], and homogenized [18].

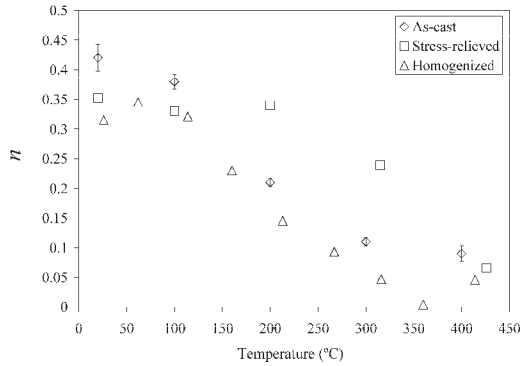

Figure 6. Strain hardening coefficient of the AA7050 alloy gained from various samples: as-cast (this study), stress relieved [14], and homogenized [18].

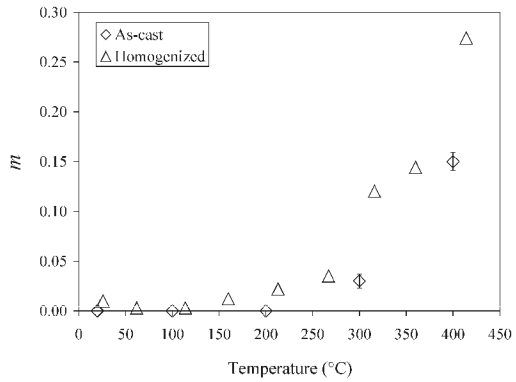

Figure 7. Strain rate sensitivity of the AA7050 alloy gained from various samples: as-cast (this study), and homogenized [18].

Computer simulations

ALSIM5 was used for the computation of temperature profile and stress/strain fields in the round AA7050 billet. Detailed description of the model can be found elsewhere [19, 20]. Geometry of the setup consisted of hot top, mold, water jet, bottom block, and the cast domain (Figure 8). New elements with the size of 0.75 mm are added to the geometry at the casting speed to simulate the continuous casting conditions. So during casting, the bottom block moves downwards while new elements are added to the system, and the mold, hot top and molten metal retain their initial position. Due to axial symmetry, only half of the billet is considered. Time-dependent thermal boundary conditions are defined to account for filling time, the air gap formation between the billet and the bottom block as well as at the billet surface, and for different heat extraction in different parts of the casting system [19]. The process parameters are listed in Table 1.

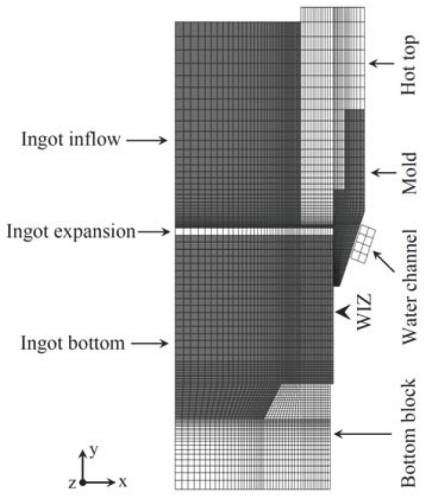

Figure 8. Geometry of the DC-cast billet used for simulations showing the hot top, mold, bottom block and the casting domain consisting of cast top (ingot inflow), cast expansion and cast bottom. Approximate position of the water impingement zone (WIZ) is also indicated on the billet surface [5].

Table I. Description of casting process parameters.

Process parameter	Value
Ingot diameter (mm)	200
Final length of the billet (mm)	380
Casting speed (mm/s)	1
Melt temperature (°C)	680
Water flow rate (l/min)	80
Water temperature (°C)	15
Start temperature of bottom block (°C)	20

Thermophysical properties of the alloy were gained from the thermodynamics database JMat-Pro provided by Corus-Netherlands (IJmuiden). The temperature dependence of the coefficient of thermal expansion, specific heat, heat conductivity, fraction solid, density and kinematic viscosity were extracted and embedded in the model. The solidification range as well as the liquidus and the non-equilibrium solidus were determined using DSC tests. Tensile mechanical properties, constitutive parameters and the K_{Ic} values of the as-cast AA7050 samples obtained from the experiments mentioned in the previous section were utilized in the model. A new module was introduced to ALSIM5 by means of which critical crack sizes could be calculated for the desired crack type and geometry based on the given K_{Ic} values and the maximum principal stress component.

Simulation results and discussion

Casting simulation was performed for 380 seconds to make sure that the steady-state conditions are gained and stress analysis can be done. After this moment, the stresses remained more or less unchanged until changes in the thermal boundary conditions were applied or casting ceased. As can be seen in Figure 9a, the lower part of the billet has reached temperatures below 80 °C.

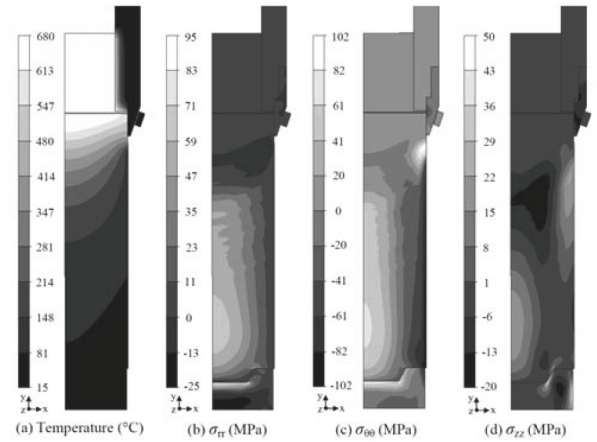

Figure 9. Computer simulation results showing the contour maps of: (a) temperature, and normal residual thermal stresses in b) radial, c) circumferential and d) axial direction after 380 s of casting at speed 1 mm/s.

Figures 9b through 9d show the contour maps of the normal residual thermal stresses generated under steady-state casting conditions. As can be seen, the residual radial stresses displayed in the lower part of the billet (on the top of the bottom block) are compressive which turn to tensile as we move in the positive "y" direction. Along the radial axis (x-axis), radial stress diminishes from 71 MPa to 3 MPa as we move towards the surface. Similar trend is observed for the circumferential stress, but it turns to compressive in the vicinity of the surface (71 MPa in the center, and –86 MPa at the surface; Figure 9c). Contour map of the axial stress (along "y" axis) follows the same trend in the lower part of the billet, i.e. tensile stresses in the center and compressive stresses at the surface. This, changes in the upper part of the billet where we see compressive stresses below the high temperature zone of the billet and tensile stresses around the water impingement area (Figure 9d). It is important to note that the circumferential stress at the surface passes through a transition from tensile to compressive as soon as the surface leaves the water impingement zone (WIZ). The tensile stresses in the WIZ reach the highest value (100 MPa) among the stresses formed in the billet.

To be able to discuss the failure probability in the billet the contour maps of the three components of the principal stress tensor ($\sigma_{33}<\sigma_{22}<\sigma_{11}$) are shown in Figures 10a, b, and c. In agreement with the results shown in Figure 9 the principal stress components appear to be tensile in the center of the billet and compressive at the surface.

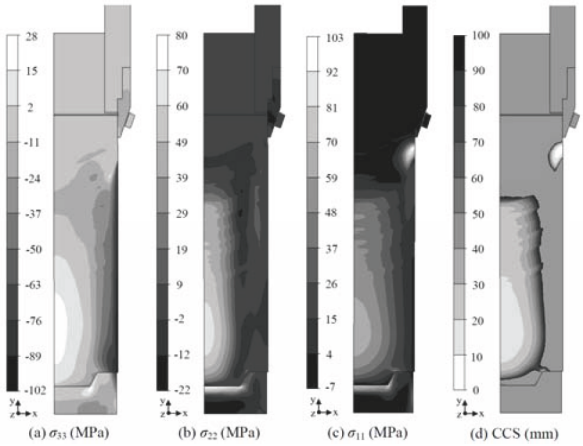

Figure 10. Computer simulation results showing the components of the principal stress tensor: (a) σ_{33}, (b) σ_{22}, and (c) σ_{11} after 380 s of casting at speed 1mm/s. (d) Critical crack size distribution for a penny shaped crack calculated using σ_{11}.

As discussed by Boender *et al.* [11], although having three tensile principal stress components in the center results in a nearly zero equivalent von Misses stress, it does not imply that no failure may occur. In other words, such a stress state facilitates the occurrence of a brittle fracture in the center of the billet. According to Rankine's theory which is more applicable to brittle materials, failure occurs when either the maximum principal stress reaches the tensile strength or the minimum principal component reaches the uniaxial compressive strength [21]. As the stresses computed by ALSIM are far below the tensile strength of the material (225 MPa at 200°C to 266 MPa at room temperature), the effect of stress raisers (cracks and flaws) should be taken into account. Similarly, in a brittle material and under a triaxial state of stress cracks mainly orient themselves normal to the largest component of the principal stresses (σ_{11}). Hence, the maximum principal stress component was selected for calculation of the critical crack sizes. A penny shaped crack was chosen as a 3D crack resembling the actual void shape in billets. For such a crack the critical crack size (radius of the penny) can be calculated as follows [5]:

$$a_c = \frac{\pi}{4}\left(\frac{K_{Ic}}{\sigma}\right)^2 \qquad (2)$$

The calculated critical crack sizes are shown in Figure 10c, with most critical locations in the center as well as the WIZ.

Validation of the simulation predictions

In order to check the validity of the cold cracking criterion, a newly developed high strength 7xxx aluminum alloy, which is highly prone to both hot and cold cracking, was selected. The material was cast in the form of a 260-mm diameter billet at Corus-Netherlands (IJmuiden) through DC casting with a conventional mold (without hot top) from the melt that was degassed in the furnace. Constitutive parameters, mechanical properties and the plane strain fracture toughness of the material were determined following the same procedures mentioned for AA7050. The mechanical properties of the new alloy resemble that of AA7050 except for the fact that the new alloy exhibits more plasticity at 200°C and the K_{Ic} values are higher compared to AA7050. The thermophysical properties of the material were obtained from the JMat-Pro database provided by Corus-Netherlands. Finally, mechanical as well physical properties databases were prepared to be implemented in ALSIM5 for thermomechanical simulations and calculation of critical crack sizes. A 260-mm diameter billet, cast at 1 mm/s with water flow rate of 35 l/min was taken as the standard case. Casting speed and water flow rate were varied to study the effect of these variables on the cracking propensity (Table II).

Table II. Description of the casting process parameters for the Ø 260-mm billets.

case	Casting speed (mm/min)	Water flow rate (l/min)
1	60 (1 mm/s)	35
2	80 (1.3 mm/s)	35
3	110 (1.8 mm/s)	90
4	60 (1 mm/s)	70

As in many cases the billets fracture at the end of casting when they are in the complete solid state, it is wise to adjust the simulation conditions in such a way that resemble the ones during the failure of the billets in practical situations. To achieve this, the casting conditions were set as follows: 1 – the first 500 s of all simulations was performed under standard conditions (case 1), 2 – changes in casting speed or water flow rate were applied afterwards by ramping up from case 1, 3 – the billet was cast then with new parameters for another 500 s, 4 – eventually, the casting speed was ramped down to zero and the billet was cooled down to room temperature over 200 s.

Contour maps of the σ_{11} are shown in Figure 11 for the cases described in Table II. In Figures 11b,c and d, the lower parts of the billets correspond to the initial casting conditions and the upper parts to the new conditions. With increasing the casting speed, the σ_{11} increases in the centre of the billet (Figures. 11a through 11c). The increase in the magnitude of the σ_{11} is due to the increased heat input mainly in the axial direction (–y) resulting in higher temperature gradients in that direction [22]. Water flow rate has a negligible effect on the magnitude of the σ_{11} and the simulation results of the billet cast with 70 l/min water flow rate (Figure 11d) are very similar to Figure 11a.

Figure 12 shows the contour maps of the CCS distribution in billets cast under conditions described in Table II. As expected, increasing the casting speed leads to smaller CCS values in the center of the billet, which means higher failure probability (Figures 11a through c). In agreement with our results in Figure 11d, the water flow rate has a negligible effect on the crack size (Figure 12d).

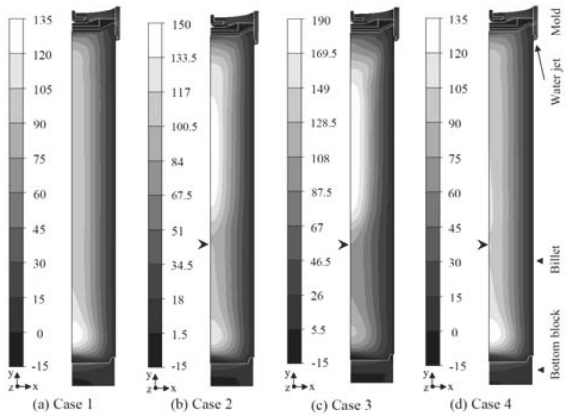

Figure 11. Simulation results showing the σ_{11} (MPa) in the billets cast at various conditions mentioned in Table II. Arrows show the transition between casting regimes [23].

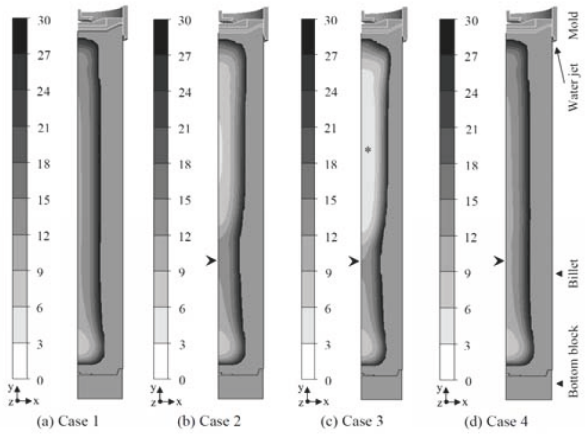

Figure 12. Simulation results showing the critical crack size distribution (mm) in the billets cast at various conditions mentioned in Table II. Crack sizes larger than 30 mm are neglected and appear as gray between the billet surface and the black area at mid-radius [23]. Arrows show the transition between casting regimes and the star in (c) indicates the location of the inclusion which triggered the catastrophic failure.

DC-casting trials were performed for the cases mentioned in Table II to check the simulation results. No cracks were observed in cases 1, 2 and 4. A real cold crack however occurred in case 3 during the casting with an audible bang resulting in the failure of the billet. According to Figure 12c, in the center of the billet cracks or defects with a critical diameter 6 to 12 mm (3 to 6 mm in radius) may lead to catastrophic failure. Further investigation of the fracture surface in case 3 revealed an inclusion with a length of 7 mm, which was located 20 mm away from the center of the billet and 730 mm above the bottom block (Figure 13). The predicted critical crack size (the diameter of the penny) for the coordinate mentioned above is 7.5 mm, which is 0.5 mm longer than the actual observed void. The reason for such a deviation

might be the fact that the actual crack shape is more complicated and irregular than the simplified penny shaped crack. In reality, cracks have sharper edges that may approach that of an ideally sharp crack.

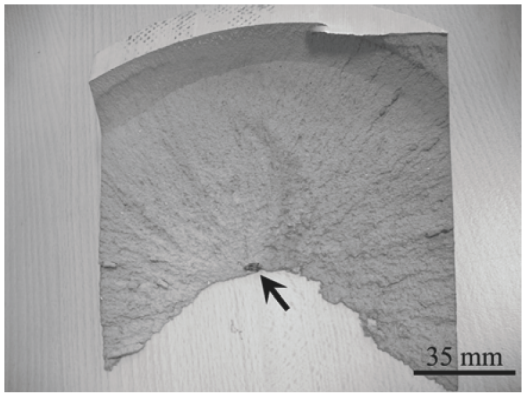

Figure 13. The cold crack surface in the billet cast at 110 mm/min and water flow rate of 90 l/min. The dark point shown by an arrow triggered the fracture. The chevron markings radiating from this oxide inclusion indicate its role in the fracture.

Conclusions

Cold cracking propensity was studied using the simulation results and casting trials on several billets under various conditions. The simulation results showed that as the casting speed increases, the CCS decreases leading to a higher failure probability of the billets. This was proven by casting trials. The critical crack sizes were validated upon experiments, where a 7 mm inclusion in the centre of the billet triggered the catastrophic failure.

Acknowledgments

This research was carried out under the project number MC4.05237 in the framework of the Research Program of the Materials innovation institute M2i (www.m2i.nl). Support of Corus (Tata Steel Europe) and Aleris is greatly appreciated. Authors would like to especially thank Dr. A. Ten Cate for the preparation of the geometry and mesh simulation files.

References

[1] J.B. Hess, "Physical Metallurgy of Recycling Wrought Aluminum Alloys", *Metallurgical Transactions A*, 14 (1983), 323-327.

[2] M. Lalpoor, D.G. Eskin, and L. Katgerman, "Microstructural Features of Intergranular Brittle Fracture and Cold Cracking in High Strength Aluminum Alloys", *Materials Science and Engineering A*, 527 (2010), 1828-1834.

[3] B. Hannart, F. Cialti, R. Van Schalkwijk, "Thermal Stresses in DC-Casting of Aluminum Slabs: Application of a Finite Element Model", ed. U. Mannweiler, (TMS, Warrendlae, PA, 1994), 879-887.

[4] J. Campbell, *Castings* (Oxford, United Kingdom: Butterworth-Heinemann, 1991), 242-245.

[5] M. Lalpoor, D.G. Eskin, and L. Katgerman, "Cold Cracking Assessment in AA7050 Billets during Direct-Chill Casting by Thermomechanical Simulation of Residual Thermal Stresses and Application of Fracture Mechanics", *Metallurgical and Materials Transactions A*, 40 (13) (2009), 3304-3313.

[6] M. Lalpoor, D.G. Eskin, and L. Katgerman, "Fracture Behavior and Mechanical Properties of High Strength Aluminum Alloys in the As-Cast Condition", *Materials Science and Engineering A*, 497 (2008), 186-194.

[7] J.R. Davis, *ASM Specialty Handbook: Aluminium and aluminium alloys*, (Materials Park, Ohio: ASM international, 1994), 68-75.

[8] V.A. Livanov, "Casting of Large Ingots for Sheet Production from Aluminum Alloys", A.F. Belov and G.D. Agarkov Eds., (Paper presented at Aluminum Alloys, Oborongiz, Moscow, 1955), 128-168.

[9] J.-M. Drezet, M. Rappaz, and Y. Krähenbühl, "Thermomechanical Effects during Direct Chill and Electromagnetic Casting of Aluminum Alloys, Part II: Numerical Simulation", ed. J. Evans, (TMS, Warrendale, PA, 1995), 941-950.

[10] K,-M. Chang, B. Kang, "Cracking Control in DC-Casting of High Strength Aluminum Alloys", *Journal of the Chinese Institute of Engineers*, 22 (1) (1999) 27-42.

[11] W. Boender et al., "Numerical Simulation of DC-Casting; Interpreting the Results of a Thermo-mechanical Model", ed. A.T. Tabereaux, (TMS, Warrendale, PA, 2004), 679-684.

[12] O. Ludwig et al., "Modeling of Internal Stresses in DC-Casting and Sawing of High Strength Aluminum Alloys Slabs", ed. C.-A. Gandin and M. Bellet, (TMS, Warrendale, PA, 2006), 185-192.

[13] J. Wan et al., "As-Cast Mechanical Properties of High Strength Aluminum Alloy", ed. B. Welch, (TMS, Warrendale, PA, 1998), 1065-1070.

[14] K.-M. Chang et al., "Computer Simulation of Solidification Cracking in High Strength Aluminum Alloys: Basic Concepts and Approach" (Paper presented at the 2nd International Conference on Quenching and the Control of Distortion, Cleveland, Ohio 4-7 November 1996), 341-345.

[15] W.M. van Haaften, "Constitutive Behavior and Hot Tearing during Aluminum DC Casting", (Ph.D. thesis, Delft University of Technology, 2002), 5.

[16] M. Lalpoor, D.G. Eskin, and L. Katgerman, "Constitutive Parameters, Mechanical Properties and Failure Mechanism in DC-Cast AA7050 Billets" (Paper presented at the 12th Intern. Conf. on Fracture, Ottawa, Canada, 12-17 July 2009).

[17] B. Magnin, L. Katgerman, and B. Hannart, "Physical and Numerical Modeling of Thermal Stress Generation during DC Casting of Aluminum Alloys", eds. M. Cross and J. Campbell, (Paper presented at MCWASP VII, TMS, Warrendale, PA, 1995), 303-310.

[18] W. M. van Haaften, (Internal report, Corus Ijmuiden, The Netherlands, 2002).

[19] H.G. Fjær, A. Mo, "ALSPEN-A Mathematical Model for Thermal Stresses in Direct Chill Casting of Aluminum Billets", *Metallurgical Transactions B* 21 (6) (1990) 1049-1061.

[20] D. Mortensen, "A Mathematical Model of the Heat and Fluid Flows in Direct Chill Casting of Aluminum Sheet Ingots and Billets", *Metallurgical and Materials Transactions B*, 30 (1) (1999) 119-133.

[21] J.H. Faupel and F.E. Fisher, *Engineering Design*, (New York (NY): John Wiley & Sons, Inc., 1981), 242-252.

[22] J.F. Grandfield and P.T. McGlade, "DC casting of Aluminum: Process Behavior and technology", *Materials Forum* 20 (1996) 29-51.

[23] M. Lalpoor et al. "Application of a Criterion for Cold Cracking to Casting High Strength Aluminum Alloys", *Materials Science Forum* 654-656 (2010) 1432-1435.

Essential Readings in Light Metals: Cast Shop for Aluminum Production.
Edited by John F. Grandfield and Dmitry G. Eskin.

Recommended Reading

Bachowski, R., and R.E. Spear. Ingot shell formation (1975, pp. 111–118).

Brobak, T.J., et al. Mathematical predictions of center crack formation in D.C. casting of aluminium billets (1991, pp. 869–876).

Dassel, J.L., and T.C. Zinniger. Sheet ingot casting with in.atable wiper (1982, pp. 793 –802).

Droste, W., and W. Schneider. Laboratory investigations about the influence of strating conditions on butt curl and swell of DC cast sheet ingots (1991, pp. 945–952).

Fjaer, H.G., et al. Coupled stress, thermal and fluid flow modelling of the start-up phase of aluminum sheet ingot casting (1999, pp. 743–748).

Giron, A., M.G. Chu, and H. Yu. Effect of mushy zone mechanical properties on the calculated stresses and deformations during the casting of an aluminum alloy ingot (2000, pp. 579–584).

Grandfield, J.F., C.J. Davidson, and J.A. Taylor. Application of a new hot tearing analysis to horizontal direct chill cast magnesium alloy AZ91 (2001, pp. 895–901).

Håkonsen, A. A model to predict the steady state pull-in during DC-casting of aluminium sheet ingots (1997, pp. 675–682).

Hannart, A., F. Cialti, and R. van Schalkwijk. Thermal stresses in DC casting of aluminium slabs: Application of a finite element model (1994, pp. 879–887).

Henrikesen, B.R., and E.K. Jensen. Modelling the effect of casting speed and metal level on the surface segregation of AA5182 (1993, pp. 969–977).

Mariaux, S., et al. Modelling of thermomechanical effects during the start-up phase of the electromagnetic casting process (1992, pp. 175–187).

M'Hamdi, M., and A. Mo. Microporosity and other mushy zone phenomena associated with hot tearing (2002, pp. 709–716).

Mo, A., et al. Modelling of surface segregation development during DC casting of rolling slab ingots (1997, pp. 667–674).

Thévoz, P., M. Rappaz, and J.L. Desbiolles. 3-MOS: A general FEM code for the prediction of microstructures in castings (1990, pp. 975–984).

Weaver, C.H. An empirical model to explain cross-section changes of D.C. sheet ingot during casting (1976, pp. 441–456).

Yu, H. A process to reduce DC ingot butt curl and swell (1980, pp. 613–628).